Concurrent validity of embedded solutions for whole body dynamics analysis

Maxime Sabbah, Bruno Watier, Raphael Dumas, Maxime Gautier, Vincent Bonnet

Concurrent validity of embedded solutions for whole body dynamics analysis

Maxime Sabbah, Bruno Watier, Raphael Dumas, Maxime Gautier and Vincent Bonnet

***Abstract*— This study investigates the possibility of estimating body segment inertial parameters (BSIP) and performing human dynamics analysis using embedded sensors. Affordable embedded inertial measurement units and instrumented force-sensing insoles have not yet demonstrated sufficient accuracy for dynamic assessments of motions in sports or rehabilitation tasks when compared to laboratory-grade solutions, such as marker based stereophotogrammetric systems and force plates. In this paper, we developed a BSIP identification pipeline to estimate inertial parameters among ten healthy young volunteers. Once these parameters are properly identified, several comparisons can be made. First, for the external wrench, we compare estimates derived from different kinematic modalities coupled with either identified BSIP or anthropometric tables against force plate measurements. Second, for joint torques, we compare estimates using embedded kinematics and either identified BSIP or anthropometric tables to the best available reference, which comes from marker-based stereophotogrammetric systems combined with identified BSIP. For validation, in the Y-Balance postural test, comparing external wrench estimates using kinematics from embedded inertial measurement units and identified BSIP to force plate measurements revealed a root mean square error of 5.9N for forces and 18.0N.m for moments, which corresponds to a large center of pressure position error of 3.2cm. Overall, using identified BSIP reduced the normalized root mean square error for joint torques by 6.5% compared to using anthropometric tables, suggesting that kinematic errors from embedded inertial measurement units cannot be entirely compensated.**

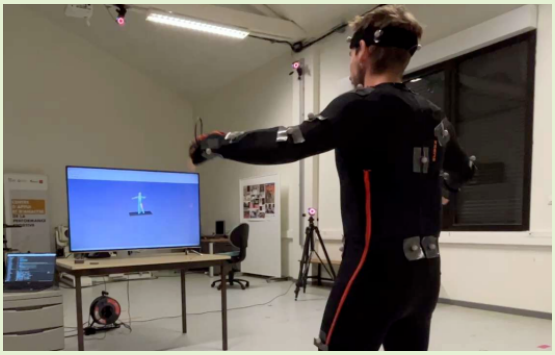

***Index Terms*— Body Segment Inertial Parameters, Embedded sensors, Inverse dynamics**

I. Introduction

ASSESSMENT of human dynamics through the analysis of joint torques, external wrenches, or center of pressure has become standard practice for informed decision-making in various fields, including biomechanics, orthopedics, ergonomics, and robotics. One way to estimate these quantities is through inverse dynamics, which requires kinematic and dynamometric measurements coupled with a human model and body segment inertial parameters (BSIP). In laboratory settings, these measurements are typically conducted using marker-based stereophotogrammetric systems and force plates (FP), which are considered gold-standard tools due to their accuracy but are also cumbersome and expensive. To enhance human motion capture outside the laboratory, wearable technologies such as inertial measurement units (IMUs) and embedded force-sensing insoles have been proposed. Several studies have evaluated the accuracy of IMUs, using both commercial [28] and open-source solutions [1]. Overall, these studies report an average root mean square error (RMSE) of about 10°, though with considerable variations depending on the investigated joint [27], [28]. Upper limb joint angles estimation accuracy is lower than that of lower limb joints. The error stems from both the technology itself and, to a greater extent, the calibration of the biomechanical model. Recent work has shown that, after removing calibration offsets, joint angle errors for lower limbs can be reduced to about 5°, even during prolonged tasks [1]. However, differences in calibration procedures can lead to constant calibration offsets of segment poses. When considering inaccuracies in sensor-to-segment calibration, the RMSE for upper limb joint angle estimation can reach up to 25° [4]. Embedded force-sensing insoles can be used to assess external wrenches at ground level during ambulatory movements. Despite the variety of sensor types, which complicates the generalization of accu-

This paper has been accepted for publication on October 15, 2024, n° 76576-2024.R1. This research received no specific grant from any funding agency in the public, commercial, or not-for-profit sectors. (Corresponding author: Maxime Sabbah.)

M. Sabbah and V. Bonnet are with the Laboratoire d'Analyse et d'Architecture des Systèmes, CNRS, Université de Toulouse, 31031 Toulouse, France (e-mail:, msabbah@laas.fr; vbonnet@laas.fr)

B. Watier is with the Laboratoire d'Analyse et d'Architecture des Systèmes, CNRS, Université de Toulouse, 31031 Toulouse, France and also with the CNRS-AIST JRL (Joint Robotics Laboratory), IRL AIST Tsukuba Headquarters and Information Technology Collaborative Research Center (AIST Tsukuba Central 1), 1-1-1 Umezono, 305-8560, Tsukuba, Ibaraki, Japan (e-mail: bwatier@laas.fr).

R. Dumas is with the Laboratoire de Biomécanique et de Mécanique des Chocs, UMR T_9406, Université Gustave Eiffel, Université Claude Bernard Lyon 1, F-69622, Lyon, France (e-mail: raphael.dumas@univ-eiffel.fr).

M. Gautier is with the Laboratoire des Sciences du Numérique de Nantes, Université de Nantes, faculté des Sciences et Techniques, 44322, Nantes, France (e-mail: maxime.gautier@univ-nantes.fr).

racy analysis, state-of-the-art insoles demonstrate an average accuracy of 55N for vertical force and 1.2cm for center of pressure during walking [6], [9], [24]. For tasks where both feet are continuously held on the ground, unlike walking, force data may dissipate through areas of the insoles without sensors [9]. Furthermore, embedded insoles only capture the ground reaction force perpendicular to the contact and its corresponding moments.

The use of embedded IMUs for human dynamics analysis has been extensively studied in the literature [11], [12], [14], [21], [22], [31]. While the most common way to estimate human dynamics lies in inverse dynamics, other techniques based on forward dynamics and optimal control, as shown by Dorschky et al. [12], or data-driven methods relying on neural networks trained with various type of sensors [36], offer alternative solutions. However, the metrics used to evaluate embedded solutions in this context varied, leading to contradictory findings. Some research concluded that IMUs are not yet mature enough for reliable human dynamics analysis [11], [14], while others have shown promising results [21], [22], [31]. Diraneyya et al. [11] used IMUs for whole-body inverse dynamics during walking, jumping, and lifting, observing an average RMSE of 28.7N for vertical ground reaction force estimation. However, no conclusive statement was made regarding the accuracy of joint torque estimation. In contrast, Karatsidis et al. [21], using a musculoskeletal model and IMUs, reported an average RMSE between estimated and FP-measured external wrench of 49.2 ± 14.0N and 10.7 ± 4.7N.m. It was 28% lower in average when using reference motion capture. These differences lead to a relatively large average normalized RMSE of 24.8 ± 8.9% for lower limb joint torques. Khurelbaatar et al. [22] evaluated the accuracy of IMUs and instrumented pressure insoles for estimating joint torques and ground reaction forces during low-speed gait where inertia effects are weak. When compared to FP measurements, ground reaction forces showed an average normalized RMSE of 10%, while joint torques varied from 10.2% for lower limbs to 35.2% for the elbows. They attributed the joint torque errors to the predicted components of ground reaction forces that are unmeasured by the insoles and to IMUs joint kinematics errors. Faber et al. [14] used a commercially available IMU suit and insoles to estimate lumbar joint torques during manual lifting, reporting a high average RMSE of 30N.m, primarily due to inaccuracies in the IMUs system's estimation of segment poses. Lastly, Tan et al. [31] applied IMUs and deep neural networks to 2D knee joint kinetics estimation during walking with a normalised RMSE of 10%, suggesting robustness to changes in IMUs positions and orientations. Further validation is needed for more complex whole-body models.

In studies using embedded sensors for human dynamics analysis, the influence of BSIP is often overlooked, with researchers typically relying on averaged values from anthropometric tables [10], [12], [13], [26]. However, these values are inadequate for individuals with atypical body mass distributions [3]. Several studies [23], [26] emphasized that using anthropometric tables for joint torque estimation can result in inaccuracies of up to 20% during gait activities.

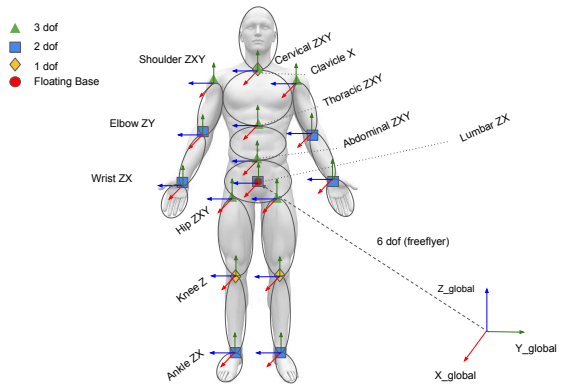

Fig. 1: The human biomechanical model description.

Thus, practical tools for identifying human-specific BSIP have been proposed. Venture et al. [2], [32], [34] devised methods using marker-based optical motion capture and FP data, combined with visual feedback, to guide participants in performing specific motion trajectories. This approach allows for the identification of the so-called base parameters, which regroup equations formed by the only observable BSIP, in a least square sense. These methods have enabled accurate estimation of external wrenches with an average RMSE of 5N and 5N.m [19]. However, one limitation of theses studies is that the identified BSIP may lack physical meaning, such as resulting in negative masses or inertia matrix that are not definite positive. To overcome this, Jovic et al. [20] used constrained quadratic programming formulations to estimate physically consistent BSIP. More recently, Werling et al. [37] proposed the AddBiomechanics tool as an add-on to OpenSim, which uses bi-level optimisation to retrieve, among others, a set of BSIP at the base of the model. They claim to reach an improved accuracy on external wrench measurements and on joint torque estimates when compared to OpenSim state-of-the art methods. However, contrary to the previous approaches, this pipeline is not real-time, as processing takes approximately 30 minutes.

In this context, the objectives of this paper are, when using fully embedded sensors, for other tasks than gait to:

- assess the feasibility to estimate joint torques and ground reaction forces and moments,
- determine the feasibility of estimating individual-specific full sets of BSIP
- understand the influence of identified instead of anthropometric tables based BSIPs on inverse dynamics outcomes.

II. Methodology

A. Biomechanical and identification models

The biomechanical model used in this study is composed of $N_s = 16$ body segments, including the pelvis, abdomen, thorax, head, left and right upper arms, lower arms, hands, upper legs, lower legs and feet and $N_j = 46$ degrees of freedom joints, as illustrated in Fig. 1 . The relative pose of each segment in the kinematic chain, as well as the rotation sequences, were defined according to the recommendations of the International Society of Biomechanics [40], [41]. The floating base, located at the pelvis segment, was positioned

within a universe coordinate system R_0 using three prismatic and three revolute joints. The orientations of the segments, expressed as quaternions $\mathbf{q}_s^0 \in \mathbb{R}^{4\times N_s}$, along with their positions $\mathbf{p}_s^0 \in \mathbb{R}^{3\times N_s}$ and the positions of the joints $\mathbf{p}_j^0 \in \mathbb{R}^{3\times N_j}$ were estimated using the forward kinematics model f as follows:

$$\begin{bmatrix}\mathbf{p}_s^0 & \mathbf{q}_s^0 & \mathbf{p}_j^0\end{bmatrix} = \mathrm{f}(\boldsymbol{\theta}, \mathbf{L}) \tag{1}$$

where $\boldsymbol{\theta} \in \mathbb{R}^{N_j}$ and $\mathbf{L} \in \mathbb{R}^{N_s}$ are the vectors of joint angles and segments lengths, respectively. Dynamic identification aims to estimate a total set of $N_{\text{BSIP}} = 10 \times N_s$ BSIP. For each segment $j \in [1, N_s]$, they are referred to as $\boldsymbol{\Phi}_j = [M_j \ \mathbf{MS}_j \ \mathbf{TI}_j]$, expressed in the joint frame, where M_j is the mass, $\mathbf{MS}_j = [MSX_j \ MSY_j \ MSZ_j]$ is the 3D vector of the first moment of inertia, and the 6D vector $\mathbf{TI}_j = [XX_j \ YY_j \ ZZ_j \ XY_j \ XZ_j \ YZ_j]$ encompasses the elements of the 3×3 tensor of inertia. Gautier [17] demonstrated that any vector of dynamometric measurements $\mathbf{Y} \in \mathbb{R}^{N_j}$ can be linearly related to the BSIP through the dynamic regressor matrix $\mathbf{W}(\boldsymbol{\theta}, \dot{\boldsymbol{\theta}}, \ddot{\boldsymbol{\theta}}) \in \mathbb{R}^{N_j \times N_{\text{BSIP}}}$. Note that $\mathbf{W}$ depends on $\boldsymbol{\theta}$ and their derivatives $\dot{\boldsymbol{\theta}}$, $\ddot{\boldsymbol{\theta}}$ which are obtained using f^{-1}, the inverse of the forward kinematic model defined in Eq. (1). We also denote as $\mathbf{J}(\boldsymbol{\theta}) = \frac{\partial \mathrm{f}}{\partial \boldsymbol{\theta}}$, the Jacobian of the forward kinematic model. For the sake of brevity, the function dependencies will not be specified further. However, due to the non-observability of all BSIP in a least squares sense, the dynamic regressor may be rank deficient, preventing the direct retrieval of the desired inertial parameters [17]. Therefore, only a minimal set of inertial parameters, referred to as base parameters and describing the system dynamics, can be identified. These are denoted as $\boldsymbol{\Phi}_B \in \mathbb{R}^{N_B}$ and can be numerically computed from the BSIP vector $\boldsymbol{\Phi} = [\boldsymbol{\Phi}_0 \ ... \ \boldsymbol{\Phi}_{N_s}] \in \mathbb{R}^{N_{\text{BSIP}}}$ by eliminating those with negligible influence on the dynamics and grouping others according to the kinematic structure of the system. In the present study, $N_B = 164$ base parameters were computed using the QR decomposition of the regressor matrix $\mathbf{W}$. This also allowed obtaining the base regressor $\mathbf{W}_B \in \mathbb{R}^{N_j \times N_B}$. Once these relationships determined, the problem can be formulated as:

$$\mathbf{Y} = \mathbf{W}_B \boldsymbol{\Phi}_B = \begin{bmatrix}0\\ \tau\end{bmatrix} + \sum_{k=1}^{N_c} \mathbf{J}_k^{0\,T} F_k \tag{2}$$

where:

- N_c is the number of contact points of the structure with its environment,
- $\tau \in \mathbb{R}^{N_j - 6}$ is the vector of joints torques,
- $F_k \in \mathbb{R}^6$ is the vector of external wrench acting on the structure at contact point k,
- $\mathbf{J}_k^0 = [\mathbf{J}_{b_k}^0 \ \mathbf{J}_{c_k}^0] \in \mathbb{R}^{6\times N_j}$ is composed of the base link and contact link placement Jacobian matrices at contact k with respect to R_0, which were used to map F_k to the vector of generalized forces,
- $\mathbf{W}_B = [\mathbf{W}_{B0} \ \mathbf{W}_{Bc}]^T \in \mathbb{R}^{N_j \times N_B}$ is the so-called base regressor matrix. $\mathbf{W}_{B0} \in \mathbb{R}^{6\times N_B}$ is the base regressor matrix associated to the six equations of motion of the base-link.

Since joint torques cannot be directly measured on humans, an alternative approach was proposed [33] using the upper part of Eq. (2). This portion of the equation specifically addresses the dynamics of the base link, enabling the identification of base parameters without the need for direct joint torque measurements and external wrench distribution at each contact point. Consequently, to estimate the base parameters, only measurements of the total contact external wrench F_k, along with the joint angles $\boldsymbol{\theta}$ and their derivatives $\dot{\boldsymbol{\theta}}$, $\ddot{\boldsymbol{\theta}}$, were required. Then, to obtain the least squares estimation of $\boldsymbol{\Phi}_B$, denoted as $\boldsymbol{\Phi}_B^* \in \mathbb{R}^{N_B}$, the ordinary least squares formulation was adopted:

$$\boldsymbol{\Phi}_B^* = (\mathbf{W}_{B0}^T \mathbf{W}_{B0})^{-1} \mathbf{W}_{B0}^T \mathbf{Y}_0 \tag{3}$$

with $\mathbf{Y}_0 = \sum_{k=1}^{N_c} \mathbf{J}_{b_k}^{0\,T} F_k$ the external wrench measurements vector at the base. Considering that the regressor $\mathbf{W}_{B0}$ of the linear system from Eq.(2) is a deterministic one, and the modeling error $\boldsymbol{\rho} = \mathbf{Y}_0 - \mathbf{W}_{B0}\boldsymbol{\Phi}_B$ is a zero mean Gaussian noise, the covariance matrix $\mathbf{C} \in \mathbb{R}^{N_B \times N_B}$ of the estimation error of $\boldsymbol{\Phi}_B^*$ was computed as follow:

$$\mathbf{C} = \mathbb{E}((\boldsymbol{\Phi}_B - \boldsymbol{\Phi}_B^*)(\boldsymbol{\Phi}_B - \boldsymbol{\Phi}_B^*)^T) \tag{4}$$

where $\mathbb{E}$ is the expectation operator. Let $c_{i,i}$ be the diagonal elements of $\mathbf{C}$ and Φ_{Bj}^* the j-th element of $\boldsymbol{\Phi}_B^*$, the relative standard deviation $\sigma_{\Phi j\%}$ is given by:

$$\sigma_{\Phi j\%} = 100 \frac{\sqrt{c_{i,i}}}{\Phi_{Bj}^*} \tag{5}$$

At last, from the estimation of $\boldsymbol{\Phi}_B$, it was possible to derive the estimation of physically consistent BSIP $\boldsymbol{\Phi}$ [20]. To achieve this, a constrained quadratic programming formulation was used. The objective of this problem was to identify the inertial parameters enforced to remain physically plausible by constraints while simultaneously fitting the dynamometric measurements and staying close to their nominal values. [3], [20]:

$$\begin{aligned}
\text{Find} \quad & \boldsymbol{\Phi}^* = \underset{\boldsymbol{\Phi}}{\operatorname{argmin}} \ \alpha\|\mathbf{Y} - \mathbf{W}\boldsymbol{\Phi}\|^2 + (1-\alpha)\|\boldsymbol{\Phi}_{AT} - \boldsymbol{\Phi}\|^2 \\
\text{s.t.} \quad & M_j > 0 \\
& 0 \leq \mathbf{MS}_j - M_j \mathbf{CoM}_j^- \\
& \mathbf{MS}_j - M_j \mathbf{CoM}_j^+ \leq 0 \\
& \text{for } v \neq 0, v^T \mathbf{TI}_j v > \epsilon
\end{aligned} \tag{6}$$

where $\boldsymbol{\Phi}_{AT}$ was the nominal vector of inertial parameters given by anthropomorphic tables for human [13]. $\mathbf{CoM}_j^+$ and $\mathbf{CoM}_j^-$ denoted the upper and lower 3D boundaries on the position of the center of mass for link j, respectively. Those boundaries have been determined using each participant's body segments geometry. $v \in \mathbb{R}^{2000\times 3}$ consisted of 2000 non zero vectors uniformly distributed over the unit sphere used to enforce the positivity of the inertia matrix [20], with a tolerance parameter of $\epsilon = 10^{-3}$. $\alpha = 0.33$ is the Pareto front parameter aiming to get a minimal error on the external wrench while keeping coherent BSIP. This parameter has been evaluated empirically and was set the same for every participants. All the modeling described is this section was implemented using the robotics C++ library Pinocchio [7].

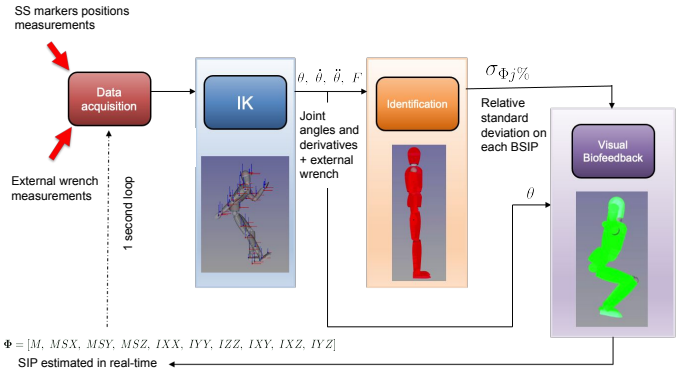

Fig. 2: Realtime closed loop identification pipeline.

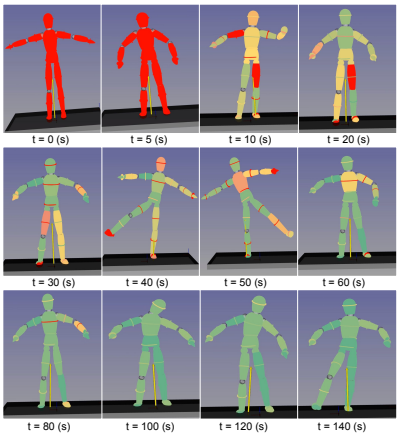

Fig. 3: Evolution of colored visual feedback during a trial.

B. Visual biofeedback

A closed-loop pipeline (Fig. 2) was proposed for the participants to generate themselves through an iterative visual biofeedback exciting motion [3]. During the experiment, a color variation, based on the values of the relative standard deviation $\sigma_{\Phi j\%}$ [35], from red to green was displayed to inform the volunteers about how well each segment was identified. The participant could then recognize which links required stimulation. The loop update rate was set to 1 second. A parameter with a $\sigma_{\Phi j\%}$ lower than 10% was considered well identified. However, for parameters with small values, such as those of the hand, they could exhibit a large $\sigma_{\Phi j\%}$ even if well identified. In such cases, if the value of the base parameter remained steady for more than 10 estimations, the associated segment was considered well identified. These results were visualized, as shown in Fig. 3, using a 3D representation of the human model defined in (II-A). Two indicators were displayed on the model: the color of the segment itself associated with centers of mass, and a little colored circle around each segment indicating the estimation of the inertia parameters.

C. Participants

Ten (7 male and 3 female) healthy adults (age: 27.4 ± 4.1yrs; height: 1.73 ± 0.07m; mass: 71.6 ± 12.3kg) performed various self-produced exciting motions using the proposed visual biofeedback (see Section II-B). No motions were specifically prescribed and the participants were free to move all their limbs in all direction at a natural pace, as long as a sufficient amount of data was collected to perform BSIP identification. They were instructed to keep at least one foot in contact with the ground and to avoid any dynamic impact on the force sensing devices. After the dynamic idenfication process was performed, they were asked to perform a Y-balance test (YBT) [8] for cross-validation. The YBT is a widely-used test for assessing postural balance, known for its simplicity, reliability, and accuracy in rehabilitation settings. During the YBT, participants stand on one leg while reaching as far as possible with the other leg in three directions: anterior, posterolateral, and posteromedial. Therefore, the whole body joint torques during the YBT will be used to cross validate the results of this study and to evaluate the effect of both the kinematics and the inertial parameters on the dynamics [38]. This investigation conforms to the principles outlined in the Declaration of Helsinki for experiments involving humans [39], and participants provided written informed consent prior to participating.

D. Equipment

Participants were equipped with embedded insoles and the 17 IMUs MVN Link suit (Xsens Technologies). Concurrent validity was assessed by comparing the kinematic data obtained from a marker-based stereophotogrammetric system composed of 22 cameras (Vero v2.2, Vicon) and FP data (AMTI OR6 Series). 35 reflective markers were attached to the Xsens suit following the Vicon Plug-in-Gait template [15] and IMU sensors placements followed the manufacturer's guidelines [30], see Fig 4.a. As depicted in Fig. 4.b, the used insoles embedded 10 piezo-resistive pressure sensors measuring plantar pressure. All the sensors were calibrated

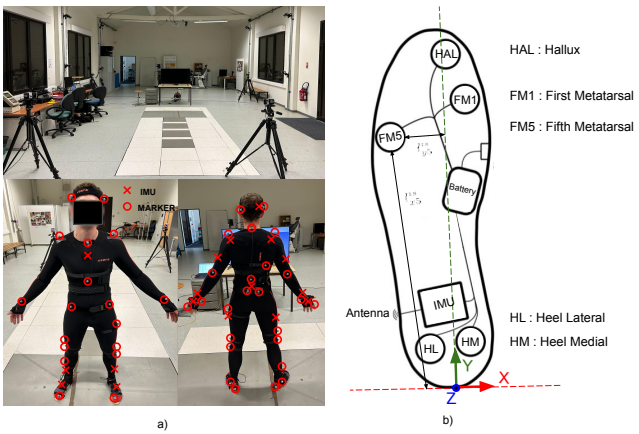

Fig. 4: a) Experimental set-up description. b) Embedded insoles description.

to fit FP data using a classical linear least squares approach [25]. The present paper examines four different modalities: one using kinematics from stereophotogrammetric systems and the anthropometric tables for BSIP denoted as SS_{AT}; one using kinematics from IMUs and the anthropometric tables for BSIP denoted as IMU_{AT}; one using kinematics with identified BSIP from stereophotogrammetric systems denoted as SS_{ID}; and one

using kinematics with identified BSIP from IMUs denoted as IMU_{ID}. Data of all systems were synchronously acquired at a frame rate of 50 Hz. All data were filtered using a Butterworth filter (5-th order, cut-off frequency of 10 Hz).

III. Results

Table I (respectively, Table V in supplementary material) presents the average RMSE and a Pearson correlation coefficient *r* calculated across all participants when comparing external wrench components during the identification (respectively, cross-validation) trials: antero-posterior (AP), medio-lateral (ML) and vertical (V) for the forces and sagittal (S), frontal (F) and transverse (T) for the moments measured by the FP and those reconstructed using the different modalities. The last column of Table I shows the comparison between force data from the insoles and the FP, revealing very large differences. For external wrench estimations during identification (respectively cross-validation) trials, SS_{ID} yielded an average RMSE of 3.8N, 5.9N.m (respectively 3.8N, 10.1N.m) for forces and moments. When using SS_{AT}, it showed an average RMSE of 5.9N and 14.4N.m (respectively 4.1N, 11.6N.m). For IMU_{ID}, average RMSE of 5.8N and 10.6N.m (respectively 5.9N, 18.0N.m) were observed whereas, for IMU_{AT}, average RMSE were of 9.1N and 23.0N.m (respectively 7.0N, 20.7N.m). Fig.5 illustrates a representative estimate of the external wrench obtained across modalities, with corresponding average RMSE of 8.6N and 16.6N.m for SS_{AT}, 5.1N and 7.1N.m for SS_{ID}, 11.4N and 23.6N.m for IMU_{AT} and 5.4N and 9.5N.m for IMU_{ID}. Fig. 6 presents the difference in value between the BSIP identified using stereophotogrammetric system kinematics and BSIP either identified using IMUs kinematics or either calculated from anthropometric tables. Table II compares the measured and estimated across modalities center of pressure position during cross-validation trials. One can note that SS_{AT} results in an average RMSE reduction of 50% when compared to IMU modalities. Table VI and Fig. 8 in supplementary material illustrate the differences between whole body joint angles estimated by IMUs and by SS chosen as reference during cross-validation, revealing an average RMSE of 13.9°. Lastly, Tables III and IV and Fig. 7 evaluate the impact of kinematics and BSIP estimates on whole-body joint torques during cross-validation. Since they cannot be measured, reference joint torques were estimated from SS_{ID} using the external wrench measured by the FP. The comparison was made for joint torques estimated with the three other modalities, using the external wrench estimated by each modality for inverse dynamic. Results are shown for the leg in contact with the ground (support leg), the trunk and both arms. Fig. 7 shows RMSE of 10.9, 15.7, 15.2N.m, NRMSE of 14.9, 27.5, 26.2% and a *r* of 0.96, 0.92, 0.94, respectively for SS_{AT}, IMU_{AT}, IMU_{ID} during a cross-validation trial for one person. For the whole body, SS_{AT} presented average normalised RMSE of 26%, whereas IMU_{AT} showed average normalised RMSE of 41% and IMU_{ID} showed average normalised RMSE of 35%.

IV. Discussion

The first objective of this paper was to investigate the possibility of using embedded sensors to perform human

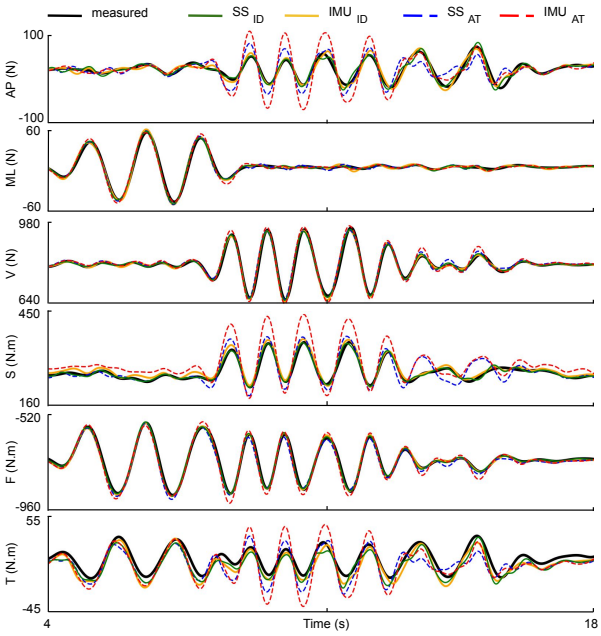

Fig. 5: Ground reaction wrench measured (black) and reconstructed with SS_{ID} (green, RMSE = 5.1N and 7.1N.m, r = 0.98), SS_{AT} (dashed blue, RMSE = 8.6N and 16.6N.m, r = 0.88), IMU_{AT} (dashed red, RMSE = 11.4N and 23.6N.m, r = 0.86), and IMU_{ID} (orange, RMSE = 5.4N and 9.5N.m, r = 0.97) for one volunteer.

TABLE I: Average RMSE and *r* between measured and estimated external wrench (AP = antero-posterior, ML = medio-lateral, V = vertical, S = sagittal, F = frontal, T = transverse) across modalities during identification trials.

-	-	SS_{AT}	IMU_{AT}	SS_{ID}	IMU_{ID}	INSOLES
AP	RMSE[N]	6.1 ± 2.5	7.7 ± 2.4	3.4 ± 1.4	5.4 ± 2.5	-
	r	0.72 ± 0.10	0.64 ± 0.12	0.92 ± 0.03	0.80 ± 0.09	-
ML	RMSE[N]	5.2 ± 1.5	9.9 ± 3.1	3.8 ± 1.3	5.8 ± 3.1	-
	r	0.98 ± 0.01	0.92 ± 0.06	0.99 ± 0.00	0.97 ± 0.03	-
V	RMSE[N]	6.5 ± 3.0	7.7 ± 3.3	4.2 ± 2.4	6.1 ± 2.8	126.2 ± 37.3
	r	0.96 ± 0.02	0.93 ± 0.05	0.98 ± 0.01	0.94 ± 0.04	0.27 ± 0.22
Mean	**RMSE[N]**	$\mathbf{5.9 \pm 2.1}$	$\mathbf{9.1 \pm 2.8}$	$\mathbf{3.8 \pm 1.6}$	$\mathbf{5.8 \pm 2.7}$	$\mathbf{126.2 \pm 37.3}$
	r	$\mathbf{0.89 \pm 0.04}$	$\mathbf{0.83 \pm 0.06}$	$\mathbf{0.96 \pm 0.01}$	$\mathbf{0.91 \pm 0.05}$	$\mathbf{0.27 \pm 0.22}$
S	RMSE[N.m]	21.5 ± 6.5	26.4 ± 11.7	4.3 ± 1.8	9.9 ± 3.8	121.6 ± 32.8
	r	0.88 ± 0.06	0.73 ± 0.14	0.99 ± 0.01	0.92 ± 0.05	0.25 ± 0.27
F	RMSE[N.m]	12.4 ± 3.6	30.5 ± 17.0	6.3 ± 2.7	13.0 ± 7.0	104.0 ± 29.1
	r	0.99 ± 0.01	0.93 ± 0.04	1.0 ± 0.00	0.98 ± 0.01	0.09 ± 0.35
T	RMSE[N.m]	9.3 ± 2.9	12.0 ± 3.8	7.2 ± 2.5	8.9 ± 3.0	-
	r	0.87 ± 0.06	0.80 ± 0.05	0.97 ± 0.01	0.92 ± 0.03	-
Mean	**RMSE[N.m]**	$\mathbf{14.4 \pm 3.5}$	$\mathbf{23.0 \pm 9.3}$	$\mathbf{5.9 \pm 2.2}$	$\mathbf{10.6 \pm 4.6}$	$\mathbf{112.8 \pm 30.9}$
	r	$\mathbf{0.91 \pm 0.03}$	$\mathbf{0.82 \pm 0.07}$	$\mathbf{0.99 \pm 0.00}$	$\mathbf{0.94 \pm 0.03}$	$\mathbf{0.17 \pm 0.31}$

dynamics analysis for estimating joint torques and center of pressure position. The first conclusion is that embedded insoles cannot be used for human dynamics analysis. As evident from the last column of Table I, the discrepancies between the FP and insoles measurements are too large. Although such insoles are commonly used for gait analysis [18], their accuracy reduces drastically during the stance phase [9]. As depicted in Fig. 4.b, some pressure on the insoles likely passes through the arch of the foot. Recent work from our group proposed using machine learning to infer the missing components of the external wrench [29]. While this approach shows promise, it is still unable to generalize across all types of double support motions. Consequently, FP data were used for inverse

TABLE II: Average RMSE and r between measured and estimated CoP position during YBT cross-validation trials.

-	-	SS_{AT}	IMU_{AT}	SS_{ID}	IMU_{ID}
CoP AP	RMSE [cm]	2.3 ± 0.9	3.4 ± 1.4	1.7 ± 0.5	3.4 ± 1.3
	r	0.79 ± 0.11	0.84 ± 0.06	0.85 ± 0.11	0.85 ± 0.07
CoP ML	RMSE [cm]	1.4 ± 0.4	3.7 ± 1.7	1.6 ± 0.4	3.0 ± 1.3
	r	0.90 ± 0.15	0.72 ± 0.19	0.93 ± 0.13	0.74 ± 0.19
Mean	**RMSE [cm]**	$\mathbf{1.9 \pm 0.6}$	$\mathbf{3.6 \pm 1.6}$	$\mathbf{1.6 \pm 0.4}$	$\mathbf{3.2 \pm 1.3}$
	r	$\mathbf{0.85 \pm 0.13}$	$\mathbf{0.78 \pm 0.13}$	$\mathbf{0.89 \pm 0.12}$	$\mathbf{0.80 \pm 0.13}$

TABLE III: Average RMSE, Normalized RMSE, and r between reference support leg joint torques estimated from SS_{ID} with FP measurement and those estimated using other modalities with estimated external wrench during YBT cross-validation trials.

-	-	SS_{AT}	IMU_{AT}	IMU_{ID}
Support hip	RMSE [N.m]	9.3 ± 2.5	13.9 ± 4.5	10.7 ± 3.2
	NRMSE [%]	22.4 ± 8.8	32.4 ± 13.1	25.8 ± 9.1
	r	0.93 ± 0.05	0.75 ± 0.16	0.77 ± 0.16
Support knee	RMSE [N.m]	15.3 ± 5.9	30.0 ± 16.7	33.3 ± 22.8
	NRMSE [%]	15.5 ± 6.9	34.2 ± 32.8	39.6 ± 43.3
	r	0.94 ± 0.04	0.85 ± 0.07	0.88 ± 0.07
Support ankle	RMSE [N.m]	12.8 ± 9.0	39.7 ± 20.1	36.7 ± 24.9
	NRMSE [%]	19.5 ± 10.1	50.0 ± 24.8	48.6 ± 31.5
	r	0.85 ± 0.12	0.69 ± 0.23	0.73 ± 0.23
Mean	**RMSE [N.m]**	$\mathbf{12.5 \pm 5.8}$	$\mathbf{27.9 \pm 13.8}$	$\mathbf{26.9 \pm 19.2}$
	NRMSE [%]	$\mathbf{19.1 \pm 8.6}$	$\mathbf{38.9 \pm 23.6}$	$\mathbf{35.9 \pm 21.1}$
	r	$\mathbf{0.91 \pm 0.07}$	$\mathbf{0.76 \pm 0.15}$	$\mathbf{0.79 \pm 0.15}$

TABLE IV: Average RMSE, Normalized RMSE, and r between reference upper limbs joint torques estimated from SS_{ID} with FP measurement and those estimated using other modalities with estimated external wrench during YBT cross-validation trials.

-	-	SS_{AT}	IMU_{AT}	IMU_{ID}
Lumbar	RMSE [N.m]	6.5 ± 3.0	12.4 ± 4.2	7.2 ± 2.2
	NRMSE [%]	12.1 ± 8.1	25.8 ± 13.7	14.5 ± 6.9
	r	1.00 ± 0.01	0.93 ± 0.06	0.95 ± 0.04
Abdominal	RMSE [N.m]	5.2 ± 3.1	8.3 ± 3.7	6.13 ± 3.3
	NRMSE [%]	15.9 ± 7.9	25.3 ± 12.6	18.4 ± 9.0
	r	0.94 ± 0.04	0.84 ± 0.09	0.91 ± 0.06
Thoracic	RMSE [N.m]	5.0 ± 2.3	7.9 ± 4.5	6.6 ± 3.8
	NRMSE [%]	34.4 ± 13.9	46.1 ± 28.4	32.4 ± 21.9
	r	0.87 ± 0.12	0.72 ± 0.24	0.92 ± 0.05
Mean	**RMSE [N.m]**	$\mathbf{5.6 \pm 2.8}$	$\mathbf{9.5 \pm 4.1}$	$\mathbf{6.6 \pm 3.1}$
	NRMSE [%]	$\mathbf{20.8 \pm 10.0}$	$\mathbf{32.4 \pm 18.2}$	$\mathbf{21.8 \pm 12.6}$
	r	$\mathbf{0.94 \pm 0.06}$	$\mathbf{0.83 \pm 0.13}$	$\mathbf{0.93 \pm 0.05}$
Shoulders	RMSE [N.m]	1.5 ± 0.6	2.3 ± 1.0	1.7 ± 1.1
	NRMSE [%]	31.7 ± 11.7	54.0 ± 24.3	48.3 ± 25.4
	r	0.92 ± 0.08	0.79 ± 0.19	0.81 ± 0.19
Elbows	RMSE [N.m]	0.3 ± 0.2	0.5 ± 0.3	0.6 ± 0.4
	NRMSE [%]	27.0 ± 14.6	45.0 ± 26.1	52.4 ± 30.3
	r	0.88 ± 0.11	0.29 ± 0.46	0.56 ± 0.44
Wrists	RMSE [N.m]	1.1 ± 0.4	1.1 ± 0.6	0.8 ± 0.6
	NRMSE [%]	50.0 ± 17.1	52.6 ± 29.2	42.3 ± 26.1
	r	0.91 ± 0.08	0.05 ± 0.42	0.57 ± 0.43
Mean	**RMSE [N.m]**	$\mathbf{1.0 \pm 0.6}$	$\mathbf{1.3 \pm 1.0}$	$\mathbf{1.1 \pm 1.1}$
	NRMSE [%]	$\mathbf{36.2 \pm 14.5}$	$\mathbf{50.5 \pm 26.5}$	$\mathbf{47.7 \pm 27.3}$
	r	$\mathbf{0.90 \pm 0.09}$	$\mathbf{0.38 \pm 0.36}$	$\mathbf{0.65 \pm 0.35}$

dynamics in this study.

The second objective was to assess the feasibility of identifying BSIP using IMUs. Fig. 6 shows that the estimated BSIP were relatively close in values with the anthropometric ones, especially for smaller segments. As previously shown [16], the BSIP of smaller segments minimally affect the external wrench. Thus, since the second term in the cost function of the constrained QP is a regularization term, these are only marginally modified. Furthermore, the constraints in Eq. 6 ensure physical consistency. Notably, this is evident for the masses and inertia of the trunk segment. The estimates of centers of mass based on IMU also exhibit more variation for the upper limbs. This is probably due to the lower accuracy of shoulder joint angle estimations from IMU sensors as shown in Table VI in supplementary material and in [27]. It is also due to the small influence of the upper limbs BSIP on the external wrench [16]. The true inertial parameters remain unknown, but it seems possible to estimate BSIP using IMUs and FP only for large segments, as it is the case with reference stereophotogrammetric systems. [3].

Finally, it is important to understand the influence of identified BSIP on human dynamics analysis. For the estimation of the external wrench during the identification trials, identified BSIP improved the estimation by around 45%, regardless of the kinematic modality (Table I). However, this improvement is less visible during the cross-validation trials, which exhibit different movements than those used during the identification trials (Table V in supplementary material). This is especially true for the moments, even with the reference SS system, indicating errors in the dynamic model. Likely, these errors come from the trunk and thighs which, due to their distance from the vertical axis in the YBT, significantly affect the moment estimates. Furthermore, coupled with IMUs kinematics errors, this propagates to the center of pressure position estimation with a 3cm error. This is twice as large as when using SS_{AT}. Such an error can lead to incorrect diagnostic interpretations [5]. However, a relatively inaccurate estimate of the external wrench might not be a problem if insoles allow for the estimation of the complete 6D external wrench [29] or if FP are used. In the literature, when estimating joint torques from IMU data, comparisons are systematically made between IMU_{AT} and SS_{AT}. For instance, during walking, average RMSE of 13.0 ± 4.7N.m or a NRMSE of about 10% were reported for lower limbs [21], [22]. These values align with our observations in Tables III and IV between the reference SS_{ID} and SS_{AT}. Consequently, as we choose to compare our estimate with the reference SS_{ID}, we observed approximately double these values. When using IMU_{AT}, the joint torques were badly estimated with NRMSE ranging from 35 to 50%. As shown in the Table VI in supplementary material, large kinematics errors with an average error of $13.9 \pm 8.6°$ across all joints were observed when using IMUs. Interestingly, the lowest kinematics errors observed at the trunk level correspond to the lowest errors in joint torque estimates. Similarly, the largest errors were found at the upper limb level. When observing the SS_{AT} joint torque estimates, this statement cannot be made and the errors were much less important. It can be deduced that the primary source of error is coming from the IMU joint kinematics estimate. Identifying BSIP allows to compensate for IMU kinematics errors partially to perform dynamics analysis, which is true for all dynamic quantities studied. Even if BSIP identification mitigates the impact of IMUs' joint kinematics error for the identification movements,

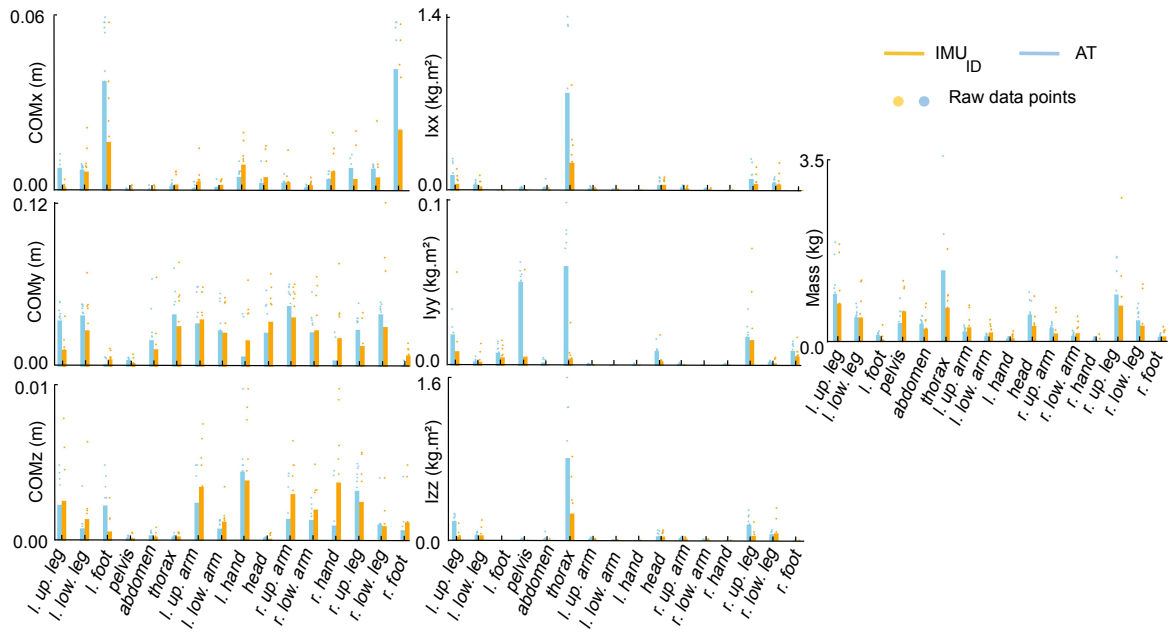

Fig. 6: Difference in values between BSIP identified with stereophotogrammetric systems and those from anthropometric tables (blue), and those identified with IMU (orange). Raw data points for all participants are shown with colored dots

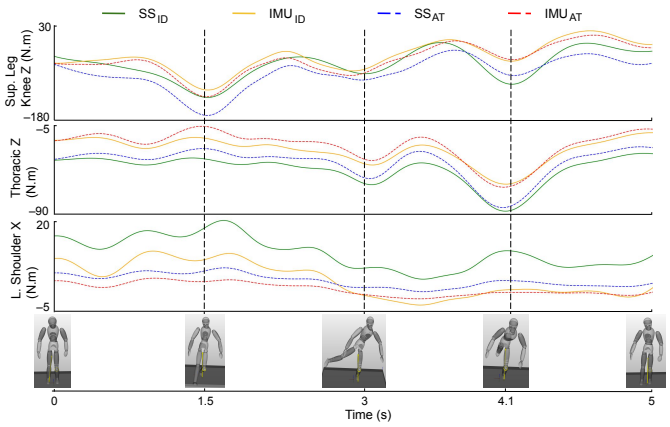

Fig. 7: Cross-validation results for joint torques estimated from SS_{ID} as reference (green), from SS_{AT} (dashed blue, RMSE = 10.9 ± 10.0N.m, NRMSE = 14.9 ± 3.3 %, r = 0.96 ± 0.04), from IMU_{AT} (dashed red, RMSE = 15.7 ± 9.7N.m, NRMSE = 27.5 ± 10.4 %, r = 0.92 ± 0.06) and from IMU_{ID} (orange, RMSE = 15.2 ± 9.4N.m, NRMSE = 26.2 ± 5.8 %, r = 0.94 ± 0.04) for one volunteer.

they cannot compensate as good the error for different cross-validation motions. Table VI exhibits very poor correlation between some joint angle estimates allowing to believe that the error in joint angle estimate is foremost due to differences in biomechanical model definition [27]. Nevetherless, joint torque estimates for lumbar and thoracic joints have been largely improved, nearly bringing IMU_{ID} performance to the level of SS_{AT}. This improvement surpasses the 40N.m RMSE that has been reported in the literature [14]. For arms' joints, RMSE values in N.m has limited meaning due to the very small amplitudes of joint torques. Khurelbaatar et al. [22] reported large NRMSE exceeding 35% when comparing to SS_{AT}. Our findings, comparing IMU_{ID} to a more accurate reference, SS_{ID}, revealed a large value of 47.7%, only 3% lower than when comparing with IMU_{AT}. However, it can be noticed that the correlation coefficients were almost twice as high for IMU_{ID} showing a much better estimate of arms joint torques.

While Khurelbaatar et al. [22] concluded that IMUs were usable for performing human dynamics analysis, we believe this statement warrants careful consideration. Although BSIP identification can mitigate some inaccuracies associated with embedded modalities, its impact on dynamics is not as significant as the impact of kinematics errors. Since IMU kinematics still cannot provide joint angle estimations with sufficient accuracy, we cannot conclude positively on their use in field applications. The very recent development of deep learning algorithms enable the use of IMUs in biomechanics without needing specific calibration [31], [36]. If such techniques can be extended to the whole body, the potential to allow accurate estimation of the kinematics using IMUs coupled with our BSIP identification method show promise in estimating accurate dynamics quantities with very few affordable sensors.

REFERENCES

[1] M. Al Borno *et al.*, "OpenSense: An Open-Source Toolbox for Inertial-Measurement-Unit-Based Measurement of Lower Extremity Kinematics over Long Durations," *J. Neuroeng. Rehabil.*, vol. 19, pp. 1–11, 2022.

[2] K. Ayusawa, G. Venture, and Y. Nakamura, "Identifiability and identification of inertial parameters using the underactuated base-link dynamics for legged multibody systems," *IJRR*, vol. 33, pp. 446–468, 2014.

[3] V. Bonnet *et al.*, "Optimal exciting dance for identifying inertial parameters of an anthropomorphic structure," *IEEE Trans. Robot.*, vol. 32, pp. 823–836, 2016.

[4] B. Bouvier *et al.*, "Upper limb kinematics using inertial and magnetic sensors: comparison of sensor-to-segment calibrations," *Sensors*, vol. 15, pp. 18813–18833, 2015.

[5] K. Brady, D. Kiernan, "The impact of centre of pressure error on predicted joint kinetics during cerebral palsy and typically developed gait: A clinical perspective," *J. Biomechs*, vol. 92, pp 155-161, 2019.

[6] G. T. Burns, J. Deneweth Zendler, and R. F. Zernicke, "Validation of a wireless shoe insole for ground reaction force measurement," *J. Sports Sci.*, vol. 37, pp. 1129–1138, 2019.
[7] J. Carpentier *et al.*, "The Pinocchio C++ Library – A Fast and Flexible Implementation of Rigid Body Dynamics Algorithms and Their Analytical Derivatives," In *SII*, Paris, France, 2019.
[8] N. J. Chimera, C. Smith, and M. Warren, "Injury history, sex, and performance on the functional movement screen and Y balance test," *J. Athl. Train.*, pp. 475–85, 2015.
[9] T. Cudejko, K. Button, M. Al-Amri, "Wireless pressure insoles for measuring ground reaction forces and trajectories of the centre of pressure during functional activities," *Sci. Rep.*, vol. 13, p. 14946, 2023.
[10] P. De Leva, "Adjustments to Zatsiorsky-Seluyanov's segment inertia parameters," *J. Biomechs.*, vol. 29, pp. 1223–1230, 1996.
[11] M. M. Diraneyya *et al.*, "Inertial Motion Capture-Based Whole-Body Inverse Dynamics," *Sensors* vol. 21, p. 7353, 2021.
[12] E. Dorschky *et al.*, "Estimation of gait kinematics and kinetics from inertial sensor data using optimal control of musculoskeletal models," *J. Biomechs.*, vol. 95, p. 109278, 2019.
[13] R. Dumas, L. Cheze, and J. P. Verriest, "Adjustments to McConville et al. and Young et al. body segment inertial parameters," *J. Biomechs.*, vol. 40, pp. 543–553, 2007.
[14] G. S. Faber *et al.*, "Validation of a wearable system for 3D ambulatory L5/S1 moment assessment during manual lifting using instrumented shoes and an inertial sensor suit," *J. Biomechs.*, vol. 102, p. 109671, 2020.
[15] M. Fellinger, J. Passler, and W. Seggl, "Plug-in Gait Reference Guide," *Human and Nonhuman Bone Identification*, vol. 197, pp. 227–46, 2010.
[16] S. Futamure *et al.*, "A sensitivity analysis method for the body segment inertial parameters based on ground reaction and joint moment regressor matrices," *J. Biomechs.*, vol. 64, pp. 85–92, 2017.
[17] M. Gautier, "Numerical Calculation of the Base Inertial Parameters of Robots," In *Proc. of IEEE ICRA*, Cincinnati, USA, 1990, pp. 1020–25.
[18] M. M. Gavrilović and M. M. Janković, "Temporal Synergies Detection in Gait Cyclograms Using Wearable Technology," *Sensors*, vol. 22, p. 2728, 2022.
[19] C. Hansen *et al.*, "An individual and dynamic body segment inertial parameter validation method using ground reaction forces," *J. Biomechs.*, vol. 47, pp. 1577–1581, 2014.
[20] J. Jovic *et al.*, "Humanoid and human inertia parameter identification using hierarchical optimization," *IEEE Trans. Robot.*, vol. 32, pp. 726–735, 2016.
[21] A. Karatsidis *et al.*, "Musculoskeletal model-based inverse dynamic analysis under ambulatory conditions using inertial motion capture," *Med. Eng. Phys.*, vol. 65, pp. 68–77, 2019.
[22] T. Khurelbaatar *et al.*, "Consistent accuracy in whole-body joint kinetics during gait using wearable inertial motion sensors and in-shoe pressure sensors," *Gait & Posture*, vol. 42, pp. 65–69, 2015.
[23] I. Kingma *et al.*, "Segment inertial parameter evaluation in two anthropometric models by application of a dynamic linked segment model," *J. Biomechs.*, vol. 29, pp. 693–704, 1996.
[24] M. S. Oerbekke *et al.*, "Concurrent validity and reliability of wireless instrumented insoles measuring postural balance and temporal gait parameters," *Gait & Posture*, vol. 51, pp. 116–124, 2017.
[25] J. Park *et al.*, "Flexible insole ground reaction force measurement shoes for jumping and running," In *Biorob*, Singapore, 2016, pp. 1062–1067.
[26] G. Rao *et al.*, "Influence of body segments' parameters estimation models on inverse dynamics solutions during gait," *J. Biomechs.*, vol. 39, pp. 1531–1536, 2006.
[27] X. Robert-Lachaine *et al.*, "Validation of inertial measurement units with an optoelectronic system for whole-body motion analysis," *Med. Biol. Eng. Comp.*, vol. 55, pp. 609–19, 2017.
[28] D. Roetenberg, H. Luinge, and P. Slycke, "Xsens MVN: Full 6dof human motiontracking using miniature inertial sensors," Tech. Rep. 1, Xsens Motion TechnologiesBV, 2009.
[29] M. Sabbah *et al.*, "Ground Reaction Forces and Moments Estimation from Embedded Insoles using Machine Learning Regression Models," *In IEEE RAS EMBS 10th Biorob*, Heidelberg, Germany, 2024
[30] M. Schepers, M. Giuberti, and G. Bellusci, "Xsens MVN: Consistent Tracking of Human Motion Using Inertial Sensing", Xsens Technologies B.V, 2018.
[31] T. Tan *et al.*, "IMU and Smartphone Camera Fusion for Knee Adduction and Knee Flexion Moment Estimation during Walking," *IEEE Trans. Industr. Inform.*, vol. 19, pp. 1445–55, 2022.
[32] G. Venture, K. Ayusawa, and Y. Nakamura, "Dynamics Identification of Humanoid Systems," In *Proc. CISM-IFToMM Symposium on Robot Design, Dynamics, and Control (ROMANSY)*, Udine, Italy, 2008, pp. 301–8.
[33] G. Venture, K. Ayusawa, and Y. Nakamura, "Identification of Human Mass Properties From Motion," *IFAC Proc. Vol.*, vol. 42, pp. 988–93, 2009.
[34] G. Venture, K. Ayusawa, and Y. Nakamura, "Real-Time Implementation of Physically Consistent Identification of Human Body Segments," In *Proc. IEEE ICRA*, 2011, pp. 6282–87.
[35] G. Venture *et al.*, "Modeling and Identification of Passenger Car Dynamics Using Robotics Formalism," *IEEE Trans. Intell. Transp. Syst.*, vol. 7, pp. 349–59, 2006.
[36] F. Wang *et al.*, "Estimation of Lower Limb Joint Angles and Joint Moments during Different Locomotive Activities Using the Inertial Measurement Units and a Hybrid Deep Learning Model," *Sensors*, 2023, vol. 23, 2023.
[37] K. Werling *et al.*, "AddBiomechanics: Automating model scaling, inverse kinematics, and inverse dynamics from human motion data through sequential optimization," *Plos One*, vol.18, 2023.
[38] B. R. Wilson *et al.*, "The relationship between hip strength and the Y balance test," *J. Sport Rehabil.*, pp. 445–450, 2018.
[39] World medical association declaration of Helsinki, "Recommendations guiding physicians in biomedical research involving human subjects," *Cardiovascular Research*, vol. 35, p. 456, 1997.
[40] G. Wu *et al.*, "ISB recommendation on definitions of joint coordinate system of various joints for the reporting of human joint motion–part I: ankle, hip, and spine. International Society of Biomechanics," *J. Biomechs.*, vol. 35, pp. 543-548, 2002.
[41] G. Wu *et al.*, "ISB recommendation on definitions of joint coordinate systems of various joints for the reporting of human joint motion—Part II: shoulder, elbow, wrist and hand," *J. Biomechs.*, vol. 38, pp. 981–992, 2005.

Maxime Sabbah received the degree in aerospace engineering from ISAE-SUPAERO, Toulouse in 2022 and the M.Sc degree in biomedical engineering from Imperial College London in 2021. Since 2022, he is a Ph.D. student at LAAS-CNRS and University of Toulouse.

Bruno Watier received the mechanical engineer degree from ENSAM and his Ph.D. in biomechanics in 1997. He is professor at Université de Toulouse III and develop his research at LAAS-CNRS in the Gepetto team. He is also involved with the Japanese-French Joint Laboratory for Robotics, Tsukuba, Japan.

Raphael Dumas received the engineer and M.Sc. degree in mechanics from INSA Lyon, 1998, and Ph.D. in mechanics from ENSAM in 2002. He is now Senior Researcher at University Gustave Eiffel, member of the Laboratory of Biomechanics and Impact Mechanics, Lyon.

Maxime Gautier received his Ph.D. in robotics and control engineering from University of Nantes in 1990. Since 1991, he has been a Professor in automatic control with University of Nantes. He is carrying out his research at "Institut de Recherche en Communications et Cybernétique de Nantes" (IRCCyN).

Vincent Bonnet received the M.Sc. and the Ph.D. degree in control and robotics, from University of Montpellier 2. From 2016, he was Associate Professor at University of Paris-Est Créteil. Since 2021, he is Associate Professor at University of Toulouse 3 and member of LAAS-CNRS.